J. Fluid Mech. (1993), *vol.* 257, *pp.* 97–110

A note on ciliated plane channel flow with a pressure gradient

By NIELS FINDERUP NIELSEN AND POUL S. LARSEN
Department of Fluid Mechanics, Technical University of Denmark, DK-2800 Lyngby, Denmark

(Received 6 March 1992 and in revised form 6 May 1993)

An envelope model is applied to the case of a two-dimensional channel with ciliated parallel walls. The formulation assumes identical values of the longitudinal and transverse amplitudes, frequency and wavelength of the two walls; it allows for arbitrary phase relations and arbitrary (not too small) spacing, and it includes an externally imposed pressure gradient. General results of a second-order perturbation analysis of creeping flow are presented. The time-averaged steady mean velocity may be viewed as the sum of two contributions: that of the pressure gradient (Poiseuille flow), and that of ciliary-driven motion which, owing to nonlinearities, also depends on the pressure gradient and reduces to pure streaming in the absence of a pressure gradient. For zero pressure gradient, the ratio of the streaming velocity of the channel and that of a single sheet shows the degree to which streaming is augmented or impeded by flow interaction. This ratio increases for the symplectic and peristaltic cases, but decreases for the antiplectic case, as the width of the channel decreases for fixed values of phase relation and amplitudes. The net flow arising from streaming and pressure gradient is shown as pump characteristics, and associated efficiencies are given. The results indicate that propulsion (pumping) is greatest and most effective for symplectic metachronism in ciliated channels with predominantly transverse waves, that it is nearly as good for peristaltic motion, but that it is considerably inferior for antiplectic metachronism in channels with predominantly longitudinal waves.

1. Introduction

Cilia are hair-like organelles that are found on the surface of organisms. The basic function of the cilia is to move water and in some cases mucus. Each cilium has a regular beat pattern consisting of the effective stroke in which it moves rapidly towards one side and the recovery stroke in which it moves more slowly back in the other direction in a bent position. In this 'rowing-type' beat, a steady velocity (streaming) is produced in the direction of the effective power stroke. Cilia usually occur in large numbers covering an entire surface uniformly, but they may also occur in isolated clumps or bands. If a group of cilia beats asynchronously, so that adjacent cilia are slightly out of phase, the movement gives rise to metachronal (out of phase) waves. While the periodic beating motion of the individual cilium is largely autonomous and biological it is believed that the metachronism displayed is a result of the mutual interaction of cilia through viscous forces.

According to the Knight-Jones (1954) terminology, different types of metachronism exist. Two types, the *symplectic* and *antiplectic* type, are termed *orthoplectic* since the effective stroke and the wave propagation occur in the same plane. In the symplectic type of metachronism the direction of the effective stroke is the same as that of wave propagation. In antiplectic metachronism the direction of the effective stroke is

opposite to that of wave propagation. Metachronism is termed *diaplectic*, on the other hand, if the effective stroke and the wave propagation occur at right angles to each other. Two types of diaplectic metachronism are distinguished, *dexioplectic* and *laeoplectic*, in which the effective stroke occurs toward the right and the left, respectively, of an observer looking in the direction of wave propagation.

Fluid transport due to systems of beating cilia has been analysed by two main approaches. One approach, the sublayer model, approximates each cilium by a line of force singularities (stokeslets) and the velocity field due to all cilia is then found by summing over all singularities. The model allows computation of the instantaneous or the average fluid velocity at any point inside or outside the cilia layer but applies only to widely spaced cilia. The sublayer model was initiated by Blake (1972) for the infinite plane wall and extended to the case of two parallel walls (Blake 1973). The latter case was later extended by Liron & Mochon (1976) and Liron (1978) to include the time variations in the cilia layer. The other approach, the envelope model, to be considered here, replaces the array of closely packed cilia by an envelope of cilia tip profiles whose prescribed motion as a flexible and, in general, extensible surface determines the velocity field outside the cilia layer. The model implies that the cilia totally entrain the fluid in the interstitial space and it is appropriate for many biological systems where the flow between neighbouring cilia is unimportant because of small interciliary distance. See Brennen & Winet (1977) for a summary.

Many envelope models have been made for water propulsion based on the two-dimensional waving sheet. Taylor (1951) made an inextensible model of a transverse wave at zero Reynolds number. Reynolds (1965) introduced a first-order motion in the longitudinal direction, as well as in the transverse direction, by allowing the sinusoidal surface to strain. Tuck (1968) simplified the results of Taylor and Reynolds and considered longitudinal and transverse oscillations separately. Blake (1971*b*) considered longitudinal and transverse oscillations acting together, which implied a variety of shapes of envelopes not considered previously. External flows induced by ciliated surfaces of other geometries have been considered, such as the infinite cylinder (Blake 1971*b*), travelling surface waves on a sphere (Blake 1971*a*), and then oscillating boundary layer on a sphere (Brennen 1974). The envelope model, in the long-wavelength approximation, has also been used to model various physiological flows, for example, cilia-induced flow in the female and male reproductive tracts (Lardner & Schack 1972). The two-dimensional channel flow due to transverse oscillations of the walls (peristaltic motion) (Jaffrin & Shapiro 1971) including an imposed pressure gradient was formulated by Burns & Parkes (1967) using a general perturbation analysis for creeping flow. Results, to second and fourth order in amplitude, were presented for two cases, namely the streaming due to peristaltic motion without a pressure gradient, and the flow due to a pressure gradient for a channel with fixed wavy walls. The case of peristaltic motion was later treated numerically by Takabatake & Ayukawa (1982), extending the results to finite amplitudes and moderate values of the Reynolds number. In a similar study, Takabatake, Ayukawa & Mori (1988) also evaluated the efficiency of peristaltic pumping in tubes as well as in channels.

In the present study we extend the work of Burns & Parkes (1967) on two-dimensional channel flow to include arbitrary phases of the beating cilia on the two walls and to investigate pressure gradient and streaming acting together. The motivation for studying these effects is the following hypothesis about the functioning of the pump of the blue mussel (*Mytilus edulis*) (Jørgensen 1989). Based on observations of pumping rates in the blue mussel under conditions of excessive relaxation, the normal relaxed state and disturbed states, corresponding to different

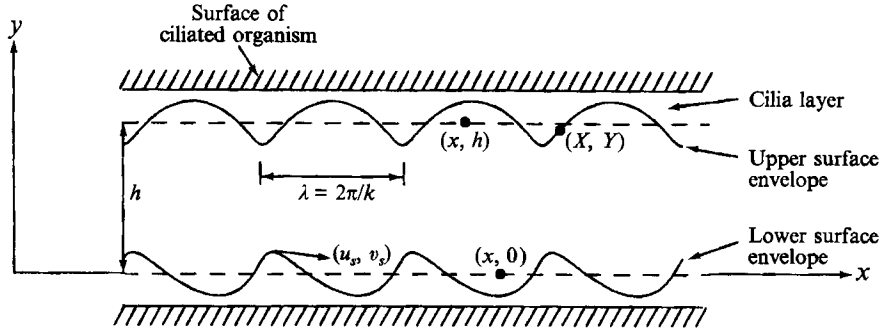

FIGURE 1. Model of a channel of nominal width h with ciliated parallel walls illustrating envelopes over cilia. Coordinates (X, Y) represent the envelope, and $(x, 0)$ and (x, h) their mean position.

widths between opposing bands of lateral cilia, it has been hypothesized (Jørgensen 1990, p. 55ff) that the distance between opposing bands of cilia has been dimensioned for the largest favourable hydrodynamic interaction in regard to pumping rate when the animal is relaxed. The pump in question is considered to be the narrow bands of lateral cilia, positioned on opposite walls of essentially two-dimensional channels formed by the gill filaments. Cilia are arranged in rows forming an angle of about $+40°$ and $-40°$ with the direction of flow, respectively, in two opposing bands whose metachronal waves are diaplectic, moving in opposite directions as the laeoplectic type. Wavefronts are probably similarly inclined. Because of the three-dimensionality and complexity of the boundary conditions of this problem we address the simpler, two-dimensional problem of a plane, ciliated channel of infinite extent with orthoplectic motion. The results of this model cannot be expected to apply to the diaplectic flow. However, our main objective is to determine the conditions for which the interaction between flows induced by the two opposing cilia systems can lead to an augmentation of the net flow. Here, the envelope model is convenient. Although limited to small amplitudes and to surfaces of infinite extent this model can provide rather general results by analytical means and is a step towards a realistic model.

As has been mentioned, the envelope model is appropriate for cilia that are sufficiently closely packed. To fully entrain the fluid in the interstitial space between cilia, their spacing d should be small compared to the viscous length (Stokes radius) ν/u or $\nu/\omega L$, where ν is the kinematic viscosity and, $u \approx \omega L$ a typical cilium velocity, ω denoting the angular frequency and L the cilium length. Also, the effect of the wall should not be felt at the tip envelope, implying $d/L < 1$. The above condition, $d < \nu/\omega L$, is sufficient for the case of symplectic metachronism where the cilium beats in the same direction as the wave is progressing and the cilia are closer together throughout the whole beat. But this is not the case for antiplectic metachronism, a conclusion reached by Blake (1972). In this case, the cilia separation at the peak of the effective stroke is increased by approximately $L \sin(kd) \approx Lkd$, assuming $kd \ll 1$, where kd is the phase between two adjacent cilia, $k = 2\pi/\lambda$ is the wavenumber, λ being the wavelength. The above criterion then becomes $d(1 + Lk) < \nu/\omega L$. The foregoing reasoning is due to Brennen (1974). He concluded less restrictively, probably because usually $Lk > 1$, that $dLk \ll \nu/\omega L$, $kd < 1$. These conditions are valid for many cilia systems (see Brennen & Winet 1977).

The envelope model is applied to a two-dimensional channel with ciliated parallel walls (figure 1). The cilium beat is represented by both symplectic and antiplectic waves, involving both longitudinal and transverse oscillations. Orthoplectic met-

achronal waves of the two walls have arbitrary phases, but the same speed and amplitude, with transverse oscillations in phase, and the channel is subject to an arbitrary pressure gradient.

2. Formulation of the problem

For creeping motion at vanishing oscillatory Reynolds number ($Re = \omega/k^2\nu$), inertia may be neglected and the two-dimensional, incompressible flow is governed by

$$\nabla \cdot \boldsymbol{v} = 0, \quad \nabla p = \mu \nabla^2 \boldsymbol{v}, \tag{1a, b}$$

where $\boldsymbol{v} = (u, v)$ denotes the velocity, p the pressure, and μ the dynamic viscosity, assumed to be constant. Here, continuity is satisfied by introducing the stream function, $u = \partial\psi/\partial y$, $v = -\partial\psi/\partial x$, and the curl of the balance of momentum becomes

$$\nabla^4 \psi = 0. \tag{2}$$

The oscillating extensible walls of the channel at $(x, y) = (X, Y)$ are defined by (see figure 1)

$$X_L = x + a \sin(z + \phi_L), \quad Y_L = b \sin z, \tag{3a}$$

$$X_U = x + a \sin(z + \phi_U), \quad Y_U = h - b \sin z, \tag{3b}$$

where L and U refer to the lower and upper surfaces respectively, a is the longitudinal and b the transverse amplitude, h the nominal channel width, ϕ the phase, and

$$z = \omega t - kx \tag{4}$$

is a convenient parameter representing a frame in which waves are stationary. Equation (4) describes progressive waves of velocity $c = \omega/k$ in the positive x-direction. One set of amplitude parameters and one frequency are appropriate and give, with two phase parameters, considerable flexibility. To limit the number of parameters no phase lag has been introduced between transverse amplitudes. From (3) it is noted that the effective beat in the ciliated surfaces occurs near $z = \frac{1}{2}\pi$. Hence, the longitudinal velocity component (see (5) below) is positive for the symplectic metachronism with $\pi < \phi < 2\pi$ and negative for the antiplectic metachronism with $0 < \phi < \pi$, and any combination of metachronisms of the two walls may be studied.

The boundary conditions are those of no slip along the walls, implying the following specified velocities at the lower and upper walls, respectively:

$$u_L = \dot{X}_L = a\omega \cos(z + \phi_L), \quad v_L = \dot{Y}_L = b\omega \cos z, \tag{5a}$$

$$u_U = \dot{X}_U = a\omega \cos(z + \phi_U), \quad v_U = \dot{Y}_U = -b\omega \cos z. \tag{5b}$$

The final condition of an externally imposed pressure gradient is needed to completely determine the volume flux through the channel. (The inverse problem of an externally imposed volume flux with the aim of determining the pressure gradient will not be considered but its solution may be inferred from the present ones.) Partial integration of (1 b) gives the longitudinal pressure increase over one wavelength,

$$\Delta p = \mu \int_0^\lambda \nabla^2 u \, \mathrm{d}x, \tag{6}$$

which may be evaluated at any value of y because of the periodic nature of the problem, see also (7) below.

3. Perturbation solution

Following the method of Burns & Parkes (1967) the stream function and the vorticity are expanded in Fourier series and the coefficients are determined from the resulting ordinary differential equations, which gives

$$\psi(z,y) = l_0 y^3 + m_0 y^2 + h_0 y + \frac{\omega}{k^2}\sum_{n=1}^{\infty}\{\sinh(nky)[(a_n + b_n ky)\sin(nz) + (c_n + d_n ky)\cos(nz)] + \cosh(nky)[(e_n + f_n ky)\sin(nz) + (g_n + h_n ky)\cos(nz)]\}. \quad (7)$$

The series solution (7) is periodic in z, higher harmonics being needed to accommodate nonlinearities introduced by the boundary conditions below, which determine the real coefficients l_0, m_0, h_0 and $a_n \cdots h_n$ to the desired order. The first two terms on the right-hand side of (7), part of the general solution to (2), are needed to accommodate the pressure gradient and differences in phase between the sheets. The y-dependence is in effect a series expansion in powers of dimensionless amplitudes ka and kb, which need be small compared to unity (see also Burns & Parkes 1967). Clearly there is no upper bound on channel width h, but we expect a lower bound, $2b < h$.

Inserting $u = \partial\psi/\partial y$ into (6) immediately yields

$$l_0 = -\frac{P}{6\mu}, \quad (8)$$

where P denotes the pressure drop per wavelength ($P = -\Delta p/\lambda$). Thus, for P to denote a pressure gradient opposing the flow driven by the ciliated walls it should be negative for symplectic metachronism but positive for antiplectic metachronism.

To approximately satisfy (5) at the actual location of the walls (3) we expand the velocity in Taylor series, from $(x, 0)$ for the lower wall,

$$\left.\begin{aligned} u(X_L, Y_L) &= u(x,0) + (X_L - x)\frac{\partial u}{\partial x}(x,0) + Y_L\frac{\partial u}{\partial y}(x,0) + \cdots, \\ v(X_L, Y_L) &= v(x,0) + (X_L - x)\frac{\partial v}{\partial x}(x,0) + Y_L\frac{\partial v}{\partial y}(x,0) + \cdots, \end{aligned}\right\} \quad (9a)$$

and from (x, h) for the upper wall,

$$\left.\begin{aligned} u(X_U, Y_U) &= u(x,h) + (X_U - x)\frac{\partial u}{\partial x}(x,h) + (Y_U - h)\frac{\partial u}{\partial y}(x,h) + \cdots, \\ \mathrm{v}(\mathrm{X_U}, \mathrm{Y_U}) &= \mathrm{v(x,h)} + (\mathrm{X_U} - \mathrm{x})\frac{\partial v}{\partial x}(x,h) + (Y_U - h)\frac{\partial v}{\partial y}(x,h) + \cdots. \end{aligned}\right\} \quad (9b)$$

Then, inserting $u = \partial\psi/\partial y$ and $v = -\partial\psi/\partial x$ from (7) into (9), equating the results to (5), and including all terms up to second order in ka and kb, yields the coefficients $a_1 \cdots h_1$, given in the Appendix, and

$$m_0 = -\tfrac{1}{2}(c/b)(a_1 + f_1 + ka\sin\phi_L), \quad (10)$$

$$h_0 = \tfrac{1}{2}c\{-(ka)^2\cos^2\phi_L - (kb)^2 + ka(a_1 + f_1)\sin\phi_L - 2kbb_1\}. \quad (11)$$

4. Results

The main interest being the net effect of the cilia-lined walls on the flow, here we focus on the resulting mean velocity. This is defined as the mean flow rate divided by mean channel width and it is calculated from (Jaffrin & Shapiro 1971)

$$U = \frac{1}{2\pi}\int_0^{2\pi}\left\{\frac{1}{h}\int_{Y_L}^{Y_U}\frac{\partial\psi}{\partial y}\,\mathrm{d}y\right\}\mathrm{d}t, \tag{12}$$

which to second order may be expressed as

$$U = l_0h^2+m_0h+h_0-\frac{cb}{2h}\{\sinh(kh)[b_1+e_1+khf_1]+\cosh(kh)[a_1+khb_1+f_1]+a_1+f_1\}. \tag{13}$$

To interpret this result it is first noted that retaining only terms to first order in amplitudes ka, kb yields $m_0 = -\frac{3}{2}hl_0, h_0 = 0$, and the last term in (13) vanishes. As expected, the solution to this order consists of linear harmonic oscillations superposed upon a Poiseuille flow driven by P, and there is no streaming. Next, to second order, cilia-driven streaming appears, but it is coupled with the pressure gradient term l_0 that enters into coefficients a_1, b_1 and f_1, hence into m_0, h_0 and the last term of (13). The streaming amounts to a constant plus a term that is linear in y whenever the two sheets are not in phase; m_0 includes contributions from this linear term and from the pressure gradient.

In the case of Poiseuille flow through a uniform channel the mean velocity is $U_P = Ph^2/12\mu$, which is also the value of the net flow U of (13) when $a = 0, b = 0$ (first-order solution). The present solutions have been evaluated for the cases reported by Burns & Parkes (1967). The results agree with their second-order solution for both peristaltic motion with no pressure gradient and for fixed wavy walls.

For the problem at hand, (13) made dimensionless by the wave velocity U/c, is a function of six dimensionless parameters: kh, ka, kb, ϕ_L; ϕ_U, and P. They represent channel width, longitudinal and transverse amplitudes, phases of metachronal waves at the lower and upper walls, and the externally imposed pressure gradient, respectively.

In view of the large number of parameters, a complete parameter study is not feasible. Attention is therefore confined to three specific waveforms with quantified amplitudes. We denote by *case 1* that of predominantly transverse waves, with $ka/kb = 0.4$ ($ka = 0.2$, $kb = 0.5$), by *case 2* that of predominantly longitudinal waves, with $ka/kb = 2.5$ ($ka = 0.5$, $kb = 0.2$), and by *case 3* that of peristaltic motion ($ka = 0$, $kb = 0.5$). For these three cases the influence of the remaining parameters on the resulting mean velocity, U/c, is studied. The influence of the channel width is given particular attention since it will reveal the mutual interaction of flows induced by two cilia systems.

4.1. *Streaming*, $P = 0$

In the absence of a pressure gradient, it is of interest to compare the present results for streaming in the channel to those for a single waving sheet, which may be calculated from

$$U_s/c = \tfrac{1}{2}[-(ka)^2+(kb)^2-2ka\,kb\sin\phi] \tag{14}$$

(see for example Brennen & Winet 1977, equation 29). For the two amplitude ratios used in the present study, (14) reduces to $\pm 0.1050-0.10\sin\phi$, where the plus and minus signs correspond to case 1 and case 2, respectively.

Results for the streaming velocity (13) versus phases are shown in figure 2 for case

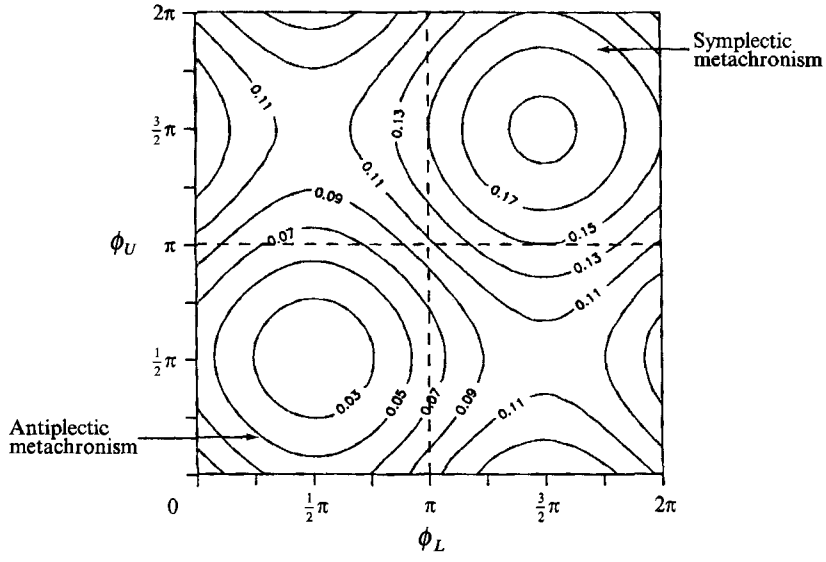

FIGURE 2. Dimensionless streaming velocity U/c at no pressure gradient versus phase angles ϕ_L and ϕ_U; case 1, $kh = 10$, $P = 0$.

1 and a large spacing of about 1.6 times the wavelength, $kh = 10$. Streaming is high when both sheets beat in symplectic metachronism (upper right quadrant of figure 2). It decreases as one sheet beats in antiplectic metachronism, and it becomes very small when both sheets beat in the antiplectic mode, clearly an inefficient combination of parameters. A map corresponding to figure 2 for case 2 proves to be that of figure 2 mirrored about the diagonal through upper left and lower right quadrants and with the sign of streaming reversed. This fact can be seen by interchanging a and b in (14), noting that the solution for large kh becomes the mean value of contributions from each sheet considered separately. Actually, numerical studies indicate that the spacing of $kh = 10$ is not quite adequate to correspond to the asymptotic case of infinite spacing between sheets.

The results in figure 2 also show that the symplectic mode is most effective for predominantly transverse waves, contrary to the antiplectic mode which is most effective for predominantly longitudinal waves. This conclusion is in agreement with the results of Blake (1971*b*) for the single waving sheet but it is found to also be valid for smaller values of the spacing for the channel. Thus, figure 3(*a*) shows case 1 and figure 3(*b*) case 2, both for spacing equal to about 0.5 times the wavelength, $kh = 3$. In figure 3(*a*) the interaction between induced flows augments the streaming with both sheets in the symplectic mode, again reaching a maximum at a common phase of $\frac{3}{2}\pi$. However, the minimum streaming, at a common phase $\frac{1}{2}\pi$ with both sheets in the antiplectic mode, is also positive and shows an augmentation relative to the case at $kh = 10$. This positive streaming for all phase relations is perhaps surprising but is a characteristic of predominantly transverse waves, culminating in peristaltic motion. Results for case 2, for $kh = 3$ (figure 3*b*), show slightly smaller streaming for pure antiplectic metachronism, becoming positive for pure symplectic metachronism. Apparently, transverse waves are relatively insensitive to the metachronism, while longitudinal waves are only effective for antiplectic metachronism.

Next, results of the streaming velocity versus non-dimensional channel width (kh) for different phase relations of surfaces defined by (3) are shown in figures 4 and 5 for

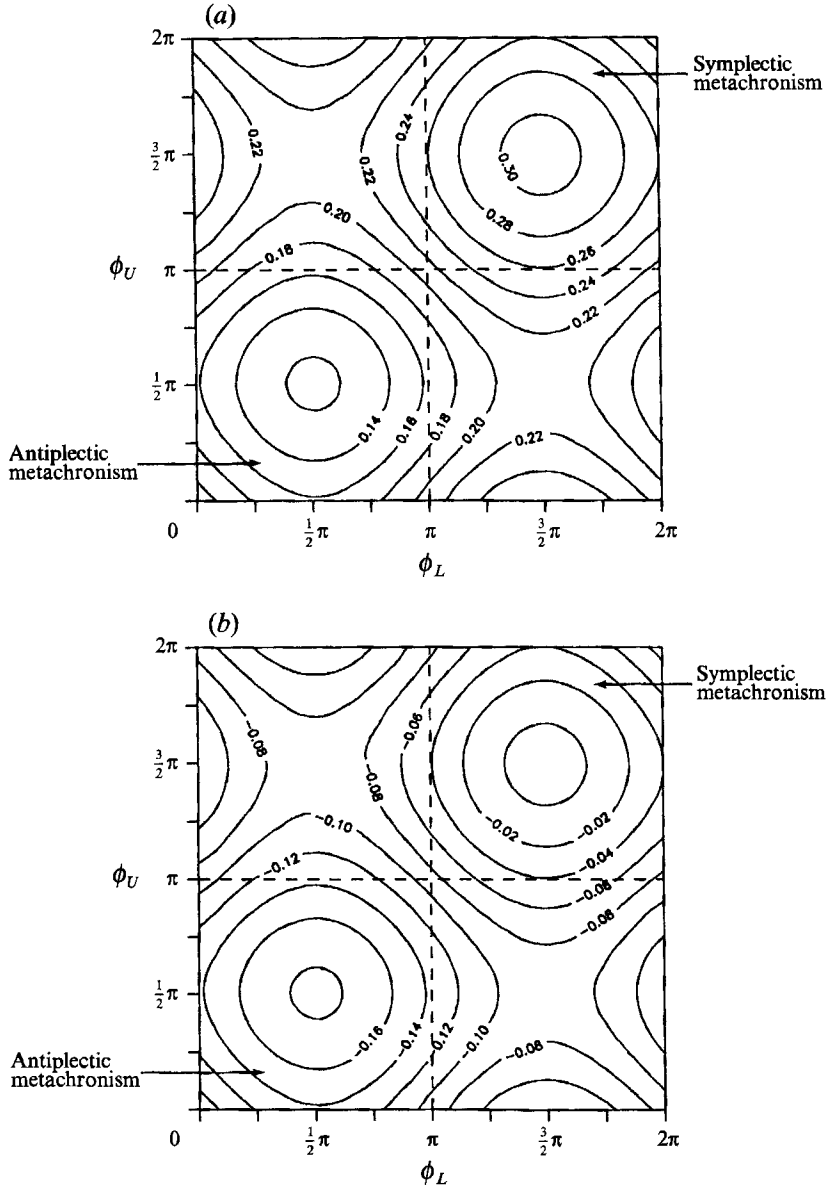

FIGURE 3. Dimensionless streaming velocity U/c at no pressure gradient versus phase angles ϕ_L and ϕ_U; (*a*) case 1 and (*b*) case 2; $kh = 3$, $P = 0$.

case 1 and case 2, respectively. Here, only ciliated channels with either symplectic or antiplectic waves on both walls are considered. For close spacing of symplectic metachronism of case 1 (figure 4) the streaming velocity in the positive x-direction *increases* as the channel width decreases. For large spacing ($kh > 5$) the streaming decreases slightly as the channel width decreases. For antiplectic metachronism of case 2 (figure 5), on the other hand, the magnitude of streaming *decreases* monotonically as the channel width decreases from infinity. Also, the magnitude of the streaming is generally greater for symplectic metachronism of case 1 than for antiplectic metachronism of case 2 for close spacing.

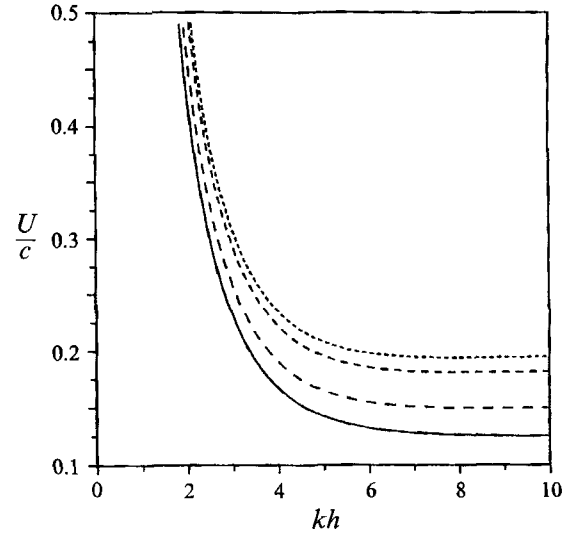

FIGURE 4. Dimensionless streaming velocity U/c at no pressure gradient versus dimensionless channel width kh for selected phase relations: symplectic metachronism of case 1 ($\phi_L = \frac{3}{2}\pi$), $P = 0$: ——, $\phi_U = \frac{3}{2}\pi$; — — — —, $\phi_U = \frac{3}{2}\pi \pm \frac{1}{4}\pi$; — · — · —, $\phi_U = \frac{3}{2}\pi \pm \frac{1}{2}\pi$; ·····, peristaltic motion of case 3 ($ka = 0$, $kb = 0.5$).

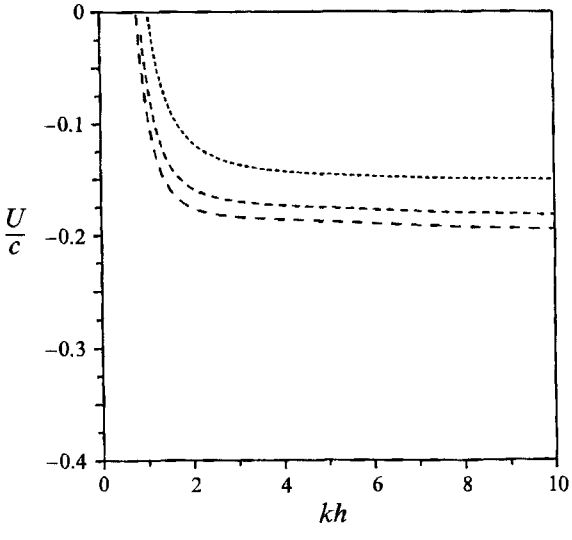

FIGURE 5. Dimensionless streaming velocity U/c at no pressure gradient versus dimensionless channel width kh for selected phase relations; antiplectic metachronism of case 2 ($\phi_L = \frac{1}{2}\pi$), $P = 0$; ——, $\phi_U = \frac{1}{2}\pi \pm \frac{1}{2}\pi$; — · — · — · —, $\phi_U = \frac{1}{2}\pi \pm \frac{1}{4}\pi$; — — — —, $\phi_U = \frac{1}{2}\pi$.

Finally, figure 4 also shows case 3 of peristaltic motion (of the same amplitude as case 1), for which the streaming is always less than for the other cases shown.

For close spacing of symplectic metachronism of case 1, the streaming velocity is greater for the optimum channel (see figure 4 for $\phi_U = \phi_L$) than for the single sheet (see (14)). For large spacing ($kh > 5$) the streaming data prove to be slightly lower (rather than greater) than the asymptotic values, which are the mean values of streaming of each sheet calculated from (14). Numerical studies indicate that this is a special feature

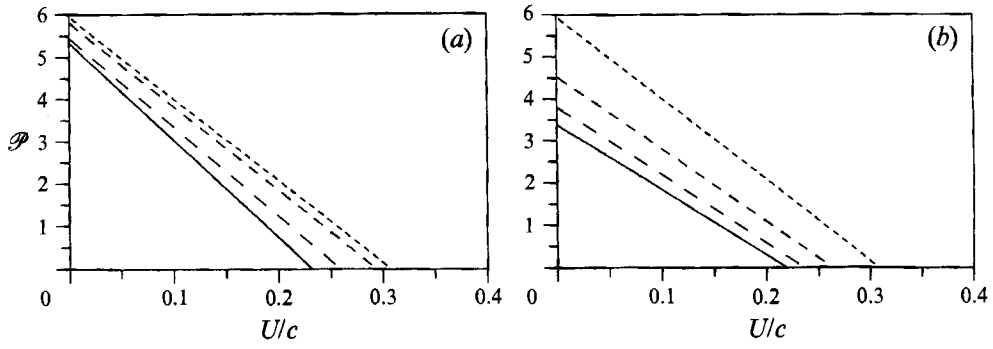

FIGURE 6. Pump head $\mathscr{P}$ versus dimensionless mean velocity U/c. (*a*) Selected phase relations of symplectic metachronism of case 1 ($\phi_L = \frac{3}{2}\pi$): ——, $\phi_U = \frac{3}{2}\pi$; — — —, $\phi_U = \frac{3}{2}\pi \pm \frac{1}{4}\pi$; — · — · —, $\phi_U = \frac{3}{2}\pi \pm \frac{1}{2}\pi$; — · · — · · —, peristaltic motion of case 3. (*b*) Selected channel widths of symplectic metachronism of case 1 with the two sheets in phase ($\phi_L = \phi_U = \frac{3}{2}\pi$); – – –, $kh = 3.0$; — — —, $kh = 3.5$, — · — · —, $kh = 4.0$; — · · — · · —, $kh = 4.5$.

of symplectic phase relations of both cases 1 and 2 and other amplitude ratios. For antiplectic metachronism of case 2, the magnitude of the streaming velocity is always smaller for the optimum channel (see figure 5 for $\phi_U = \phi_L$) than for the single sheet (see (14)). This suggests a constructive interference of the oscillating motion generated by each sheet for symplectic metachronism of predominantly transverse waves, and a destructive interference for antiplectic metachronism of predominantly longitudinal waves for narrow ciliated channels.

4.2. *Pump characteristics*

By including a pressure gradient, simulating an externally imposed flow resistance, the ciliated channel acts as a pump ($P < 0$ for symplectic metachronism and $P > 0$ for antiplectic metachronism). Figure 6 shows typical pump characteristics, in terms of non-dimensional pump head ($\mathscr{P} = -h^2 P/\mu c$) versus flow ($U/c$), calculated from (13). Figure 6(*a*) shows pump characteristics for $kh = 3$ and different phase relations of symplectic metachronism of case 1, as well as the special case of peristaltic motion, involving no phase relations. In this case, the most efficient pump is that of the two sheets in phase. Figure 6(*b*) shows the effect of channel width on the characteristics for the two sheets of symplectic metachronism of case 1 in phase. Here, the most efficient pump is clearly that with close spacing.

As expected, all pump characteristics are linear. This is readily shown by inspection of the right-hand side of (13), where c appears as the factor in all terms not involving l_0, which includes some terms contained in the coefficients a_1, b_1 and f_1 appearing in the last term of (13) (see also the Appendix). Therefore, (13) may be rearranged as an equation for the pump characteristic,

$$\mathscr{P} = A_1(A_2 - U/c), \tag{15}$$

where $\mathscr{P} = -h^2 P/\mu c$ is the dimensionless pressure rise delivered per wavelength, and constants A_1 and A_2 depend on parameters ka, kb, kh, ϕ_L, and ϕ_U. This shows the characteristics to be linearly decreasing with increasing flow, which is to be expected for a leaky viscous pump. It also shows the explicit dependence on viscosity and frequency, to be discussed below.

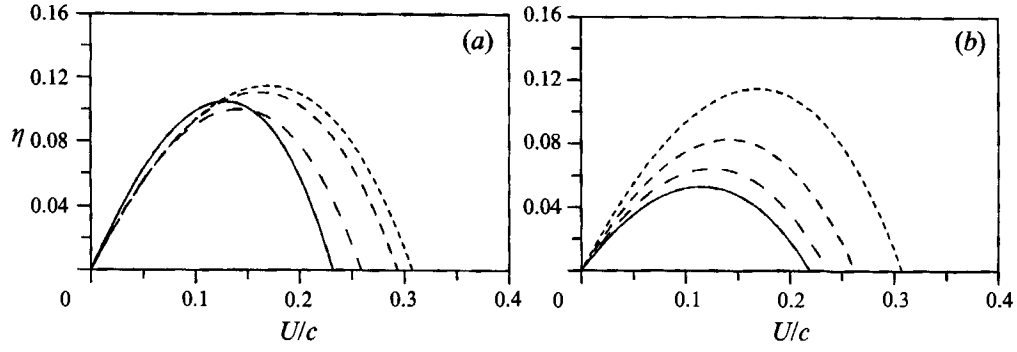

FIGURE 7. Pump efficiencies η versus dimensionless mean velocity U/c for the pumps in figure 6.

4.3. *Pump efficiency*

The mechanical efficiency η of the ciliated channel pump is defined as the ratio of useful (reversible) power hUP gained by the fluid per unit length of channel to the actual power $\dot{E}$ expended by the envelopes on the fluid (Shapiro, Jaffrin & Weinberg 1969); thus

$$\eta = -hUP/\dot{E}. \tag{16}$$

The averaged power required in working against viscous stresses and pressure per unit length of channel, accounting for the slope of envelopes, is calculated from

$$\dot{E} = \frac{1}{T}\int_0^T \frac{1}{\lambda}\int_0^\lambda [u(\tau_{yx} - \sigma_{xx}\tan\Theta) + v(\sigma_{yy} - \tau_{xy}\tan\Theta)]_{y=Y_L}^{y=Y_U}\,\mathrm{d}x\,\mathrm{d}t, \tag{17}$$

where

$$\sigma_{ij} = \tau_{ij} - p\delta_{ij}, \quad \tau_{ij} = \mu\left(\frac{\partial u_i}{\partial x_j} + \frac{\partial u_j}{\partial x_i}\right), \tag{18}$$

and the pressure along the envelopes is obtained by evaluating the integral in x of (1*b*) at $y = Y_L$ and $y = Y_U$, respectively. The slope of envelopes (3) is given by $\tan\Theta = (\partial Y/\partial x)/(\partial X/\partial x)$.

Figure 7 shows efficiencies calculated from (16), to second order in ka and kb, for the particular pump cases considered in figure 6. The symplectic pump of case 1 is seen to be superior to the peristaltic pump at high flow and relatively small pressure gradients. Numerical results indicate that the symplectic pump of case 1 is considerably superior to the antiplectic pump of case 2 in regard to performance and efficiency. Also, numerical studies indicate that it is necessary to account for the slope of envelopes for the relatively high values of amplitudes used in the present study.

5. Discussion

In this paper the envelope model has been applied to a ciliated two-dimensional channel subject to a pressure gradient. The main objective has been to determine the ciliary water propulsion dependence on channel width and phase relations of the metachronal waves of the two sheets forming the channel walls. To limit the number of parameters, transverse amplitudes were assumed to be in phase but longitudinal amplitudes could have arbitrary phase. Also, frequency, wavelength, and amplitudes were the same for the two sheets.

Creeping flow solutions have been obtained to second order in dimensionless transverse and longitudinal amplitudes, which should be small compared to unity.

Results are exemplified by specific cases of the amplitude ratio: one of predominantly transverse waves; one of predominantly longitudinal waves; and that of pure transverse waves (peristaltic pumping). The first case always provides the most effective propulsion for symplectic metachronism and the second case for antiplectic metachronism. Peristaltic motion provides good propulsion, but not the best. Some added longitudinal amplitude in symplectic metachronism has been found to yield better propulsion.

In the absence of a pressure gradient, results for the channel are compared to those of a single waving sheet to illustrate the degree to which streaming is augmented or impeded by the flow interaction. In fact, our numerical studies of the solution show that in the limit of large channel width (compared to wavelength) the streaming for the channel approaches the mean value of streaming predicted for each single sheet. This result appears to be physically meaningful although it is not readily shown from the analytical solution. As channel width is decreased, all cases of antiplectic metachronism yield a monotonically decreasing magnitude of the streaming. All cases of symplectic metachronism, however, following a small decrease, yield increasing values of streaming, and the augmentation may be manyfold for narrow channels. Of course, the streaming cannot exceed the wave velocity. These overall trends appear reasonable because decreasing channel width is expected to favour propulsion in the direction of the metachronal wave. The inversion of the effect of flow interference on net streaming (for $kh > 5$) found in all cases of symplectic metachronism studied, although very small, is puzzling and no physical explanation is at hand.

These results show some trends similar to those for a waving sheet near a wall or in a channel. For this problem, Katz (1974) found the influence of a wall to be important for $kh \leqslant 5$, which may be compared to negligible change in streaming for $kh \geqslant 5$ in our figures 4 and 5. He also found the propulsive velocity, and the power expended, to increase as the distance to the walls is decreased for the symplectic case.

By including a pressure gradient, the results have been interpreted and presented as pump characteristics and associated efficiencies. The results indicate that the most efficient pump is that of close spacing of two opposing sheets with predominantly transverse waves in symplectic metachronism and in phase. In general, for given geometry, amplitudes and wavelength, (15) also shows that the shut-off head of the present pump (P for $U = 0$) is proportional to the product of beat frequency and fluid viscosity, $\mu\omega$, and the zero-back-pressure flow (U for $P = 0$) is proportional to the beat frequency and independent of viscosity. The same dependencies are found for peristaltic pumping at larger amplitudes in the numerical study of Takabatake & Ayukawa (1982, figures 16 and 18) for Reynolds numbers ($h^2\omega/4\pi\nu$) up to about unity. It is of some interest to note, on the other hand, that experimental results for the blue mussel suggest that the shut-off head is independent of both beat frequency and viscosity, and the zero-back-pressure flow to be inversely proportional to viscosity (Jørgensen, Larsen & Riisgård 1990). As pointed out earlier, the cilia pump of the blue mussel is quite different and the present results cannot be expected to apply to this pump. Still, it would be surprising to find that orthoplectic metachronism or finite width of cilia bands should change the dependence on frequency and viscosity. It is possible that specified kinematics of the ciliary motion may not model reality, and that the force-limited model suggested by Jørgensen *et al.* (1990) would be more appropriate.

The stimulating discussions with Professor C. Barker Jørgensen in the course of this work are gratefully acknowledged.

Appendix

To second order, coefficients in (7) are given by

$$c_1 = kakh[\{-kh\tanh^2(kh)+kh\}\cos\phi_L+\{\tanh(kh)/\cosh(kh)\}\cos\phi_U]/D,$$

$$d_1 = ka[\{kh\tanh^2(kh)+\tanh(kh)-kh\}\cos\phi_L$$
$$-\{\tanh(kh)-kh\}\cos\phi_U/\cosh(kh)]/D,$$

$$D = -\tanh^2(kh)[1+(kh)^2]+(kh)^2, \quad e_1 = kb, \quad g_1 = 0, \quad h_1 = -c_1+ka\cos\phi_L.$$

The remaining coefficients a_1, b_1, and f_1 are solved by Gauss elimination of the linear system $\boldsymbol{A}\boldsymbol{x} = \boldsymbol{y}$, where

$$\boldsymbol{A} = \begin{bmatrix} a_{11} & a_{12} & a_{13} \\ a_{21} & a_{22} & a_{23} \\ a_{31} & a_{32} & a_{33} \end{bmatrix}, \quad x = \begin{bmatrix} a_1 \\ b_1 \\ f_1 \end{bmatrix}, \quad y = \begin{bmatrix} y_1 \\ y_2 \\ y_3 \end{bmatrix},$$

$$a_{11} = \cosh(kh)+1, \quad a_{12} = \sinh(kh)+kh\cosh(kh),$$

$$a_{13} = kh\sinh(kh)+\cosh(kh)+1,$$

$$a_{21} = \sinh(kh), \quad a_{22} = kh\sinh(kh), \quad a_{23} = kh\cosh(kh),$$

$$a_{31} = \tfrac{1}{2}ka\{\sin\phi_L-\cosh(kh)\sin\phi_U\}-\tfrac{1}{2}kb\sinh(kh)-kh/kb,$$

$$a_{32} = -\tfrac{1}{2}ka\{\sinh(kh)+kh\cosh(kh)\}\sin\phi_U-\tfrac{1}{2}kb\{kh\sinh(kh)+2\cosh(kh)+2\},$$

$$a_{33} = \tfrac{1}{2}ka[\sin\phi_L-\{kh\sinh(kh)+\cosh(kh)\}\sin\phi_U]$$
$$-\tfrac{1}{2}kb\{2\sinh(kh)+kh\cosh(kh)\}-kh/kb,$$

$$y_1 = -ka(\sin\phi_L+\sin\phi_U)-kb\sinh(kh)+6l_0hkb/\omega, \quad y_2 = -kb\{\cosh(kh)+1\},$$

$$y_3 = -\tfrac{1}{2}(ka)^2\{\cos^2\phi_L-\cos^2\phi_U\}+\tfrac{1}{2}(kb)^2\{\cosh(kh)+1\}+\tfrac{1}{2}kakb\sinh(kh)\sin\phi_U$$
$$+hka\sin\phi_L/b-3(l_0k/\omega)[h^2-\tfrac{1}{2}b^2].$$

REFERENCES

BLAKE, J. R. 1971*a* A spherical envelope approach to ciliary propulsion. *J. Fluid Mech.* **46**, 199–208.

BLAKE, J. R. 1971*b* Infinite models for ciliary propulsion. *J. Fluid Mech.* **49**, 209–222.

BLAKE, J. R. 1972 A model for the micro-structure in ciliated organisms. *J. Fluid Mech.* **55**, 1–23.

BLAKE, J. R. 1973 Flow in tubules due to ciliary activity. *Bull. Math. Biol.* **35**, 513–523.

BRENNEN, C. 1974 An oscillating-boundary-layer theory for ciliary propulsion. *J. Fluid Mech.* **65**, 799–824.

BRENNEN, C. & WINET, H. 1977 Fluid mechanics of propulsion by cilia and flagella. *Ann. Rev. Fluid Mech.* **9**, 339–398.

BURNS, J. & PARKES, T. 1967 Peristaltic motion. *J. Fluid Mech.* **29**, 731–741.

JAFFRIN, M. Y. & SHAPIRO, A. H. 1971 Peristaltic pumping. *Ann. Rev. Fluid Mech.* **3**, 13–36.

JØRGENSEN, C. B. 1989 Water processing in ciliary feeders, with special reference to the bivalve filter pump. *Comp. Biochem. Physiol.* **94A**, 383–394.

JØRGENSEN, C. B. 1990 *Bivalve Filter Feeding: Hydrodynamics, Bioenergetics, Physiology and Ecology*. Fredensborg: Olsen & Olsen.

JØRGENSEN, C. B., LARSEN, P. S. & RIISGÅRD, H. U. 1990 Effect of temperature on the mussel pump. *Mar. Ecol. Prog. Ser.* **64**, 89–97.

KATZ, D. F. 1974 On the propulsion of micro-organisms near solid boundaries. *J. Fluid Mech.* **64**, 33–49.

KNIGHT-JONES, E. W. 1954 Relations between metachronism and the direction of cilia beat in Metazoa. *Q. J. Microsc. Sci.* **95**, 503–521.

LARDNER, T. J. & SCHACK, W. J. 1972 Cilia transport. *Bull. Math. Biophys.* **34**, 325–335.

LIRON, N. 1978 Fluid transport by cilia between parallel plates. *J. Fluid Mech.* **86**, 705–726.

LIRON, N. & MOCHON, S. 1976 The discrete-cilia approach to propulsion of ciliated microorganisms. *J. Fluid Mech.* **75**, 593–607.

REYNOLDS, A. J. 1965 The swimming of minute organisms. *J. Fluid Mech.* **23**, 241–260.

SHAPIRO, A. H., JAFFRIN, M. Y. & WEINBERG, S. L. 1969 Peristaltic pumping with long wavelengths at low Reynolds number. *J. Fluid Mech.* **37**, 799–825.

TAKABATAKE, S. & AYUKAWA, A. 1982 Numerical study of two-dimensional peristaltic flows. *J. Fluid Mech.* **122**, 439–465.

TAKABATAKE, S., AYUKAWA, A. & MORI, A. 1988 Peristaltic pumping in circular cylindrical tubes: a numerical study of fluid transport and its efficiency. *J. Fluid Mech.* **193**, 267–283.

TAYLOR, G. I. 1951 Analysis of the swimming of microscopic organisms. *Proc. R. Soc. Lond.* A **209**, 447–461.

TUCK, E. O. 1968 A note on a swimming problem. *J. Fluid Mech.* **31**, 305–308.